Environmental Science & Technology

Article

pubs.acs.org/est

# Albedo Impact on the Suitability of Biochar Systems To Mitigate Global Warming

Sebastian Meyer,*[,†] Ryan M. Bright,[‡] Daniel Fischer,[†] Hardy Schulz,[†] and Bruno Glaser[†]

[†]Soil Biogeochemistry, Martin-Luther-University Halle-Wittenberg, Halle, Germany

[‡]Industrial Ecology Program, Department of Energy and Process Engineering, Norwegian University of Science and Technology (NTU), Trondheim, Norway

Supporting Information

**ABSTRACT:** Biochar application to agricultural soils can change the surface albedo which could counteract the climate mitigation benefit of biochar systems. However, the size of this impact has not yet been quantified. Based on empirical albedo measurements and literature data of arable soils mixed with biochar, a model for annual vegetation cover development based on satellite data and an assessment of the annual development of surface humidity, an average mean annual albedo reduction of 0.05 has been calculated for applying 30−32 Mg ha$^{-1}$ biochar on a test field near Bayreuth, Germany. The impact of biochar production and application on the carbon cycle and on the soil albedo was integrated into the greenhouse gas (GHG) balance of a modeled pyrolysis based biochar system via the computation of global warming potential (GWP) characterization factors. The analysis resulted in a reduction of the overall climate mitigation benefit of biochar systems by 13−22% due to the albedo change as compared to an analysis which disregards the albedo effect. Comparing the use of the same quantity of biomass in a biochar system to a bioenergy district heating system which replaces natural gas combustion, bioenergy heating systems achieve 99−119% of the climate benefit of biochar systems according to the model calculation.

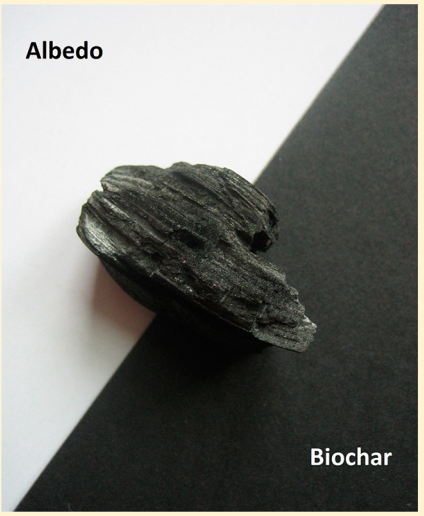


## 1. INTRODUCTION

The charring of organic matter and its application to soil with the intent to improve soil properties is known as biochar technology and commonly seen as an opportunity to mitigate global warming.[1] The carbon cycling of the charred material is slowed down compared to uncharred organic matter. In addition, the production of biochar often yields bioenergy as a coproduct which can substitute fossil fuels. Further, it was observed that the application of biochar to soil can—at least in the short term—decrease soil greenhouse gas emissions;[2−4] and increase fertilizer use efficiency.[5] Under certain conditions, there is evidence that black carbon (predominantly condensed aromatic and graphitic carbon structures which are, for example, formed during biochar production [6]) in soil can reduce the carbon mineralization of organic matter added to the soil; for example, in the form of harvest residues.[7] While all of these impacts serve to reduce radiative forcings from greenhouse gases (GHGs), there are also GHG emissions during the whole lifecycle of a biochar system starting with feedstock production up to the final degradation of the biochar in the soil (see also Meyer et al. 2011[8]). The application of biochar to soil can induce a radiative forcing[9] by changing the surface albedo (the dimensionless relation of reflected short-wave radiation to incoming shortwave radiation) and the black carbon (soot) concentration in the atmosphere.[10] Thus, there is also a risk that biochar systems might accelerate global warming.

This paper integrates the albedo impact caused by biochar application in the overall climate impact assessment of a pyrolysis-based biochar system to assess the effect of biochar systems on the climate more comprehensively. An existing, partly adapted GHG balance of a pyrolysis based biochar system compiled by Hammond et al. 2011[11] was used as basis to assess the overall climate impact of a biochar system after the integration of the albedo impact assessment. Quantifications of direct radiative forcing impacts of albedo changes when biochar is applied to soil (i.e., the increase in absorbed short-wave radiation) were based on empirical measurements and literature data. Since albedo measurements of soils mixed with biochar are still rare,[9,12] additional soil albedo measurements were carried out to strengthen the basis of the analysis. Indirect radiative forcing impacts of albedo changes (caused by changes in water vapor concentration in the atmosphere and changes in cloud cover due to changes in evapotranspiration rates resulting from changes in the ratio of latent to sensible heat fluxes) are not analyzed in this article (see also Figure 1 in Kirschbaum et

Received: June 9, 2012
Revised: October 5, 2012
Accepted: October 11, 2012
Published: November 12, 2012

  

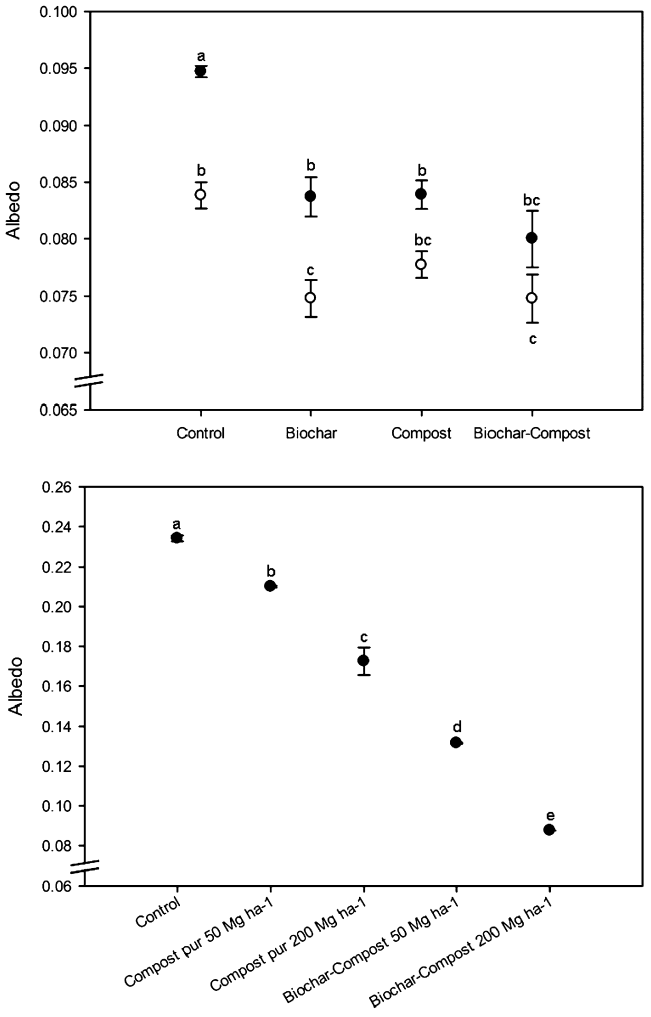


**Figure 1.** (Top) Albedo of FT soil samples before (black circles) and after (empty circles) modest drying. (Bottom) Albedo of the PT series soil samples. Significant differences of the treatment means ($p < 0.05$ with $n = 4$) are indicated by different lower case letters. Error bars indicate the standard error ($n = 4$) of the albedo values obtained from the respective treatments.

al. 2011).[13] These indirect effects are difficult to assess and were not included in the scope of the present study, although they may be, under certain conditions, quantitatively as important as the direct effect of albedo changes.[14] To stay in line with GHG metrics that integrate instantaneous radiative forcing—the instantaneous perturbation of the earth energy balance at the top of the atmosphere—caused by pulse emissions of greenhouse gases over a common time horizon, this analysis adapts a methodology applied by Bright et al. 2012[15] to express the climate impact of albedo changes in the same unit (i.e., in megagram of $CO_2$ equivalent emissions [Mg $CO_2$e]).

This paper also accounts for the climate impact caused by the temporal shift between pulse emissions of biogenic $CO_2$ during biochar production and the subsequent carbon sequestration via the regrowing biomass feedstock. A comprehensive literature review reveals that this dynamic impact has not yet been accounted for in global warming impact assessments of biochar systems.[8] In line with Cherubini et al. 2012,[32] suitable GWP characterization factors for biogenic and time-distributed $CO_2$ emissions of the biochar system under study are developed.

Results are benchmarked to the climate impact of a stand-alone bioenergy heating system which substitutes the use of fossil fuels and consumes the same amount of dry biomass feedstock as the biochar system.

## 2. MATERIALS AND METHODS

**2.1. Overview of the Modeled Biochar System.** As mentioned, we are making use of existing lifecycle GHG data of Hammond et al. 2011[11] to model the GHG balance of a biochar system consisting of a pyrolysis plant with an annual feedstock consumption of 2000 Mg biomass (25% water content) and biochar application on a wheat field. Since the results presented in section 3 are related to biochar production via slow pyrolysis, they cannot be generalized to other carbonization technologies such as fast pyrolysis, gasification, hydrothermal-, or flash carbonization. We modeled two scenarios based on two types of feedstock with different regrowth periods: Wood chips from small forestry roundwood and wheat straw. Data on GHG emissions per type of feedstock connected to the provision of biomass feedstock (including transport to the pyrolysis plants), the production of the pyrolysis plant, char transport to the field, and its application to the soil are taken directly from ref 11. Wood chips were treated as a main product, wheat straw as byproduct in the LCA inventory of this publication. We deviate from the publication in the assumptions that 55% of the energy in the synthesis gas and waste heat of the process can be supplied into a district heating system with a high annual utilization factor of 75%, that transport heat losses are 5% (see also Cholewa and Siuta-Olcha 2009,[17]) and that resulting emissions saving are 0.252 kg CO2e/kWh final energy (see UBA 2012[18]) due to the replacement of natural gas heating systems. Due to the limited scientific knowledge on a discussed positive impact of biochar application on soil inherent organic matter stabilization, such an effect was not accounted for. In addition, the impact of a potential increase in biomass production after biochar application on soil humus formation was not taken into account.

To model the biochar system, it is assumed that biochar is applied to an arable field near Donndorf close to Bayreuth in Bavaria/Germany and used for wheat and rapeseed cultivation. The simulation of the albedo impact of biochar application at this location is dealt with in Section 2.2. The impact of biogenic and time-distributed emissions and removal fluxes caused by the oxidation and stabilization of biochar, increases in fertilizer use efficiency, and soil $N_2O$ reduction are discussed in Section 2.3.

**2.2. Albedo Impact of Biochar Application.** *2.2.1. Laboratory Soil Albedo Measurements.* The following study was carried out: 16 wet soil samples (four treatments with four replicates of each treatment) were taken from a biochar field trial near Donndorf in Northern Bavaria [49°56′0.02″N, 11°31′15.77″E] on January 26, 2012 (see Supporting Information (SI) Figure S1). The A horizon of the field site consists mainly of sandy silt (Us) and of very sandy clay (Ls4). On the East side of the test field, the parent material is sand stone. In SI Table S.1, the different treatment volumes which had been already tilled 10 cm deep into the arable soil in July 2010 are described. The biochar used in the treatments of the field trial (application rate 31.5 Mg $ha^{-1}$) was produced from wood in a slow pyrolysis plant by the company CarbonTerra in

Duttenstein, Germany. The soil samples were taken from the soil surface (0−5 cm) of four randomly chosen sample sites of the respective treatments forming 4-fold replications, filled in plastic bags and transported to the micrometeorological laboratory of the University of Bayreuth. The albedo of the field trial soils samples was measured twice: One measurement per sample was carried out at the original water content of the soil samples. Subsequently, these soil samples were modestly dried in a drying oven at a temperature around 60 °C for 90 min, followed by a second soil albedo measurement of each sample. In addition to the albedo measurements, the gravimetric water content of each soil sample was analyzed.

The albedo of a second series of dry soil samples from a pot trial set up in the year 2009 (see Schulz et al. 2012[19]) was analyzed in the laboratory as well to study the impact of very high biochar and compost applications on the soil albedo. The control treatment of this series consists of washed sand from the Kiesgrube ZAPF, Weidenberg, Germany. Three further treatments are based on very high biochar and compost amendments to the washed sand as described in SI Table S2. The char used in the washed sand samples (application rates 23.5 and 93.8 Mg $ha^{-1}$ in two different treatments) was produced from hardwood by the charcoal producer Köhlerei Wiesener in Rohr, Austria in a traditional charcoal kiln.

For a full description of the measurement procedure, the uncertainties related to the measurement procedure, and the statistical method used to analyze the results, see the SI for this article.

*2.2.2. Impact of Vegetation Cover, Snow Cover, And Soil Humidity on the Surface Albedo Change.* The development of mean monthly surface albedo difference $\Delta\tilde{\alpha}_s$ between arable land with and without biochar application within a year is influenced by the average monthly surface water content, the average monthly vegetation cover, and the average monthly snow cover. We derive $\Delta\tilde{\alpha}_s$ in our simulation according to the following formula:

$$\Delta\tilde{\alpha}_s = [1 - \tilde{f}_g - \tilde{f}_{sc}]\Delta\tilde{\alpha}_{soil} \quad (1)$$

$\tilde{f}_g$ is the average monthly fraction of green vegetation and $\tilde{f}_{sc}$ is the average monthly fraction of snow cover. $\Delta\tilde{\alpha}_{soil}$ is dependent on the surface properties of the soil treatments which depend on the type of treatment, the change in surface properties over time, and the soil humidity (since water enforces irradiation absorption).

To model the annual development of the vegetation cover of wheat and rapeseed fields at our model location near Donndorf, the correlation between the fraction of green vegetation at a certain point in time $f_g$ and the scaled difference vegetation index (SDVI) as suggested by Jiang et a. 2006[20] was applied:

$$f_g = \mathrm{SDVI} = \frac{N - R - (N_s - R_s)}{N_v - R_v - (N_s - R_s)} \quad (2)$$

$R$ represents the surface reflectance averaged over visible regions ($\lambda \sim 0.6\ \mu m$) and N the surface reflectance averaged over near-infrared regions ($\lambda \sim 0.8\ \mu m$) of the spectrum. $N_s$ and $R_s$ represent the reflectance of bare soil, $N_v$ and $R_v$ represent the reflectance of dense vegetation. The bands 1 (0.62−0.67 $\mu$m) and 2 (0.84−0.87 $\mu$m) of the surface reflectance product MOD09A1 produced every 8 days by the moderate-resolution imaging spectroradiometer (MODIS) on the Terra satellite of NASA [21] over the years 2010 and 2011 was used to derive $f_g$ and $\tilde{f}_g$. Since the data set has a resolution of 500 × 500 m, the surface reflectance data from an agricultural field large enough to provide a homogeneous surface was needed to calculate $f_g$ and $\tilde{f}_g$. For this purpose, surface reflectance data of an agricultural field close to Penkun/Germany (Latitude (53° 19′ 23.46″) Longitude (14° 15′ 48.35″)) with wheat cultivation in 2010 and rapeseed cultivation in 2011 (no intertillage crops were cultivated in both years) was obtained. The data was used to simulate the development of green vegetation cover on the modeled field site near Donndorf without taking into account differences in the vegetation phenology between fields in Donndorf and Penkun.

According to the snow cover period map of Hochschule München,[22] there were 40−60 snow cover days per year in the region of Bayreuth in the average of the years 2005−2009. Based on this information, a total of 50 days with snow cover was evenly distributed over the months from December to February in the intra-annual delta albedo simulation. The impact of surface albedo changes on the snow cover period due to increased radiation absorption [23] was not accounted for in our assessment.

To account for the intra-annual variation in soil humidity and its impact on $\Delta\tilde{\alpha}_{soil}$, it was necessary to know how the humidity in the first millimeters of the soil surface of the field trial site near Donndorf develops over the year. Due to a lack of empirical data, we assumed in a simplified approach that dry surface conditions dominate on days without rainfall and wet surface conditions dominate on day with rainfall. Continuously measured rainfalls records (10 min measurement interval) for the years 2008−2011 in the Ökologisch-Botanischer Garten in Bayreuth provided by the Micrometeorological Department of the University of Bayreuth were used to derive the average amount of days with and without rainfall per month in the region of Bayreuth. For wet days, a $\Delta\alpha_{soil}$ of 0.027 between control and biochar treatments (directly after biochar incorporation in soil) was used in our annual delta albedo simulation for the field near Donndorf in line with the result from the Donndorf field trial (see Figure 1) and our assumption on the development of $\Delta\alpha_{soil}$ in time (see eq 4). In line with the results from the albedo measurements of Genesio et al.[9] in Pistoia, Italy (see SI Figure S2), a $\Delta\alpha_{soil}$ of 0.15 between control and biochar treatments (directly after biochar incorporation in soil) was used for dry days in the same simulation.

*2.2.3. Radiative Forcing and GWP from Albedo Change.* Methods for estimating GWP characterization factors from surface albedo changes are thoroughly discussed in refs 15,24, and 25. Thus only a brief description is presented here. Monthly mean instantaneous forcing from the monthly mean surface albedo change when biochar is applied can be described by the following equation:

$$\tilde{R}F_\alpha = -\tilde{R}_{TOA}\tilde{f}_{Atm.}\,\Delta\tilde{\alpha}_s \quad (3)$$

$\tilde{R}_{TOA}$ is the monthly mean downward solar flux at the top of the atmosphere (TOA) for our region (in $W/m^2$), $\tilde{f}_{Atm}$ is a two-way atmospheric transmittance parameter accounting for the monthly mean reflection and absorption of solar radiation (downward and upward) throughout the atmosphere for the same region, and $\Delta\tilde{\alpha}_s$ is the monthly mean surface albedo change of the sample area scaled to 1 $m^2$. $\tilde{R}_{TOA}$ is a function of latitude, sunset hour angle, and solar declination angle and is calculated following the methodology outlined in refs 26 and

27. $\tilde{f}_{Atm}$ is the product of two factors: The monthly mean clearness index, $K_T$, or the fraction of TOA irradiance reaching Earth's surface, and $T_a$ the monthly fraction reaching TOA after reflection at the surface. 22-year mean monthly clearness index data for our specific region are obtained from ref.[28] There is no empirical data on $T_a$ . Since $K_T$ and $T_a$ are subject to equal atmospheric conditions, we only slightly adapt $K_T$ to estimate $T_a$ by accounting for the multiple scattering and reflection of the upwelling shortwave radiation between the atmospheric layers and the surface. This is discussed in more detail in the SI. Monthly mean local instantaneous forcing is averaged over the year to obtain a single value for the annual forcing associated with biochar application.[15]

Genesio et al. 2012 [9] (see SI Figure S2) observed a rapid decline in $\Delta\alpha_{soil}$ within the first 18 months after biochar application on a test site in Pistoia which can be explained by subsurface biochar concentration, demobilization, clogging of the biochar surface with mineral particles and biochar degradation. The soil was tilled 10 cm deep in Pistoia as well as in Donndorf. In line with this observation, we assume that the average delta albedo in year 1 is 65% of the initial delta albedo value $RF_{\alpha-0}$ directly after biochar incorporation in soil and 32% of the start value in average in year 2. In this context, it should be noted that demobilized biochar, for example by wind erosion, might decrease the surface albedo in other areas than the field site. We did not account for this effect in our climate impact assessment. The albedo measurements on the site in Pistoia did not identify a statistically significant delta albedo after the second tilling operation anymore. We are taking a conservative approach by assuming that 22% of the start value is still present in year 3 after the second tilling operation. After year 3, the delta albedo is assumed to decay exponentially at the same decay rate as the biochar decays (see Section 2.3.1). Since albedo scales with forcing, the local mean annual instantaneous forcing time profile with a 1 year discretization takes the following functional form:

$$RF_{\alpha}(t) = \begin{cases} 0.65RF_{\alpha-0} & \forall\ t = 1 \\ 0.32RF_{\alpha-0} & \forall\ t = 2 \\ 0.22RF_{\alpha-0} & \forall\ t = 3 \\ RF_{\alpha}(3)\exp(-MRT^{-1}(t-3)) & \forall\ t > 3 \end{cases} \quad (4)$$

t indicates a complete annual time period (365 days). MRT is the assumed mean residence time of biochar (500 years) as indicated by Hammond et al. 2011.[11]

By averaging the local forcing impacts from the affected area over the area of Earth's surface, we get a global instantaneous forcing time profile that can now be used to benchmark against the effect of anthropogenic $CO_2$ emissions. Integrating over a defined time horizon (TH) allows us to estimate the magnitude of the albedo change forcing (in global W $m^{-2}$ yr/$m^2$) relative to that of a pulse emission of anthropogenic $CO_2$ (in W $m^{-2}$ yr/kg):

$$GWP_{albedo} = \frac{\int_0^{TH} RF_{\alpha}(t)dt}{\int_0^{TH} RF_{CO_2}(t)dt} \quad (5)$$

However, because GWP is meant to be an "emission" metric, we want to normalize albedo forcing impacts to biogenic $CO_2$ emission pulses from bioenergy and biochar production, thus rewriting eq 5 to

$$GWP_{albedo} = \left(\left(\frac{M_{FS} \times CC_{ODB} \times 1.33 \times 0.32}{M_{FS} \times C_E(44/12)}\right)\bullet \frac{\int_0^{TH} RF_{\alpha}(t)dt}{\int_0^{TH} RF_{CO_2}(t)dt}\right) \quad (6)$$

$M_{FS}$ is the dry feedstock mass, $C_E$ is the fraction of carbon in oven dry biomass oxidized used to provide bioenergy and produce biochar, and $CC_{ODB}$ is the carbon content in oven dry biomass contained in biochar. $C_E$ depends on the pyrolysis conditions (temperature and residence time). When wheat straw is the feedstock, $CC_{ODB}$ = 0 0.455 and $C_E$ is 0.533 in our scenario. When roundwood is the feedstock, $CC_{ODB}$ is 0.501 and $C_E$ is 0.499 in our scenario.[11,29] 1.33 is the mass of biochar per kg carbon in biochar in our scenario. 0.32—also a constant—is the average area (in $m^2$) covered by 1 kg biochar at a biochar application rate of 31.5−32 Mg/ha. 44/12 is a constant and is the mass of $CO_2$ produced by the combustion of 1 kg carbon.

Parametric uncertainty in the forcing calculations is discussed in Bright et al. (2012).[15] Uncertainty of the simple albedo forcing model applied in this paper is assessed in Cherubini et al. (2012) [24] who report a +2.9% forward bias of the annually averaged albedo RF at TOA when compared to outputs of a more advanced, highly parametrized plane-parallel radiative transfer model.[30,31]

**2.3. The Impact of Biogenic and Time-Distributed Emissions.** *2.3.1. Calculation of GWP Characterization Factors for Biogenic Emissions.* We follow the approach of Cherubini and colleagues [32] to estimate GWPs of biogenic $CO_2$ emissions from our modeled biochar-bioenergy system coproducing biochar and bioenergy used for the supply of heat to a district heating system. Essentially, time-distributed atmosphere-biosphere sequestration fluxes of $CO_2$ are integrated into the global carbon cycle and reconciled with pulse biogenic $CO_2$ emission fluxes occurring at a single point in time. We refer the reader to refs 15,16,24,32, and 33 for details/methodological elaboration.

For our biochar-bioenergy systems, roughly one-half of the carbon in the biomass feedstock is embodied in useable biochar ready for field application. 15% of C in biochar is oxidized at the start of the second year and the remaining 85% exponentially thereafter with a mean residence time of 500 years.[11] This rate gives us field carbon emissions from biochar oxidation as a function of time, or $e_{BC}(t)$. Carbon sequestration fluxes are linked to the biomass feedstock growth rate, $g(t)$, to which a simple Gaussian function is used, and subsequently normalized over the rotation length such that 100% of the initial carbon pulse is sequestered at the end of the rotation period. Following ref 32, the function for distributed emission and sequestration fluxes in time used to derive a single concentration time profile for distributed field emissions from biochar oxidation, $f_{BC}(t)$, takes the following form:

$$f_{BC}(t) = \int_0^t e_{BC}(t')y(t-t')dt' - \int_0^t g(t')y(t-t')dt' \quad (7)$$

where $y(t)$ is a $CO_2$ impulse response function (IRF) representing the fraction of $CO_2$ remaining in the atmosphere after a single pulse emission/pulse sequestration depending on the interactions between the atmosphere, oceans, and the

terrestrial biosphere.[34,35] This IRF $y(t)$ has the following analytic form:[36]

$$y(t) = A_0 + \sum_{i=1}^{3} A_i e^{-t/\beta_i} \quad (8)$$

where $A_0$ = 0.217, $A_1$ = 0.259, $A_2$ = 0.338, $A_3$ = 0.186, ß$_1$ = 172.9, ß$_2$ = 18.51, and ß$_3$ = 1.186. Because our system produces biochar and bioenergy jointly using the carbon in biomass, we choose to normalize all emission and sequestration fluxes to a unit pulse emission from biochar and bioenergy production which gives the following concentration profile as a function of time:

$$f_{BC/E}(t) = \frac{C_E y_{CO_2}(t)}{C_E} + \frac{C_{BC}\int_0^t e_{BC}(t')y_{CO_2}(t-t')dt'}{C_E} - \frac{(C_{BC}+C_E)\int_0^t g(t')y_{CO_2}(t-t')dt'}{C_E} \quad (9)$$

"GWP$_{bio}$" characterization factors for biogenic $CO_2$ emissions from our combined bioenergy-biochar system for any given TH can now be estimated

$$GWP_{bio}(TH) = \frac{\int_0^{TH} RF_{BC/E}(t)dt}{\int_0^{TH} RF_{CO_2}(t)dt} = \frac{\int_0^{TH} k_{CO_2} f_{BC/E}(t)dt}{\int_0^{TH} k_{CO_2} y_{CO_2}(t)dt} \quad (10)$$

where $k_{CO2}$ is the radiative efficiency of $CO_2$ in the atmosphere given a background $CO_2$ concentration of 378 ppmv.[36]

For comparison, GWP characterization factors for biogenic $CO_2$ emissions from stand-alone bioenergy production are shown in SI Table S4. These factors are applied to biogenic $CO_2$ emissions that occur upstream in the supply chain due to carbon oxidation associated with biomass procurement losses. These emissions are treated as pulses occurring in year 0. It was assumed that there are 5% (related to the feedstock) procurement losses for wheat straw and 9% (related to the feedstock) procurement losses for round wood.

*2.3.2. Calculation of GWP Characterization Factors for Avoided Fertilizer Use and Soil $N_2O$ Emissions.* In line with [11] a constant 10% decrease in N fertilizer requirement and a constant 5% decrease in P and K fertilizer requirement was assumed to result from biochar application. While Woolf et al. 2010 [37] assumed that the increase in the fertilizer use efficiency of the soil remains constant for 100 years after biochar application, we assume a more conservative time period of 20 years following char application in our model in line with Hammond et al. 2011[11]. The fertilizer reduction impact has been quantified previously by Hammond and colleagues amounting to −1.7 kg-$CO_{2e}$/odt biomass feedstock and year in terms of avoided 100 year $CO_2$-eq. emissions for biochar systems in the UK.[11] We use the UBA ProBas LCA database[18] in order to disaggregate $CO_{2e}$ into their relative GHG constituents: Anthropogenic $CO_2$, $CH_4$, and $N_2O$. These are then divided by their 100 year. GWP characterization factors indicated in ref 36 to obtain absolute values for avoided GHG emissions of type $x$ per Mg dry feedstock and year, or $e_x(t)$.

A similar approach is followed to obtain absolute avoided emission values for soil direct $N_2O$. Due to a recent publication of Kammann et al. 2012 [3] based on laboratory experiments, we deviate from Hammond et al. 2011 with our assumption that a constant 50% suppression of soil $N_2O$ emissions can be achieved for a time period of 5 years after biochar application. Taking into account earlier experiment results published by Libra et al. 2011,[2] the 50% reduction should be seen as an upper range estimate. We assumed that the reduction in soil $N_2O$ emissions decreases linearly from year 5 after biochar application to zero in year 15 after biochar application. Avoided direct soil $N_2O$ emission amount to −24.9 kg-$CO_{2e}$/odt and year in the years 1−5 under the assumptions described above.

We customized additional GWP characterization factors that take these avoided time-distributed emission savings into account. For these avoided emission scenarios, "negative" emissions $-e$ occurring at specific points in time $t'$ as single pulses (represented by the distribution $\varepsilon(t')$) are normalized to biogenic $CO_2$ emission pulses from biochar and bioenergy production using the factor $C_E$, the factor $CC_{odb}$, the constant 1000 (kg/Mg dry feedstock), and the constant 44/12 (kg $CO_2$ /kg C). Subsequently, they are convoluted with the corresponding decay function $y_x(t)$ of greenhouse gas type $x$ and integrated to obtain an atmospheric $CO_2$ concentration profile associated with the scenario. Radiative efficiencies $k_x$ of a substance $x$ from ref 13 are multiplied by the derived concentration time profiles to obtain instantaneous forcing time profiles, integrated to TH, and divided by the cumulative forcing of anthropogenic $CO_2$ for the same TH. These operations are combined to yield the following equation which is repeated for each of the avoided emission scenarios:

$$GWP_{-e_x}(TH) = \left( \frac{\int_0^{TH} k_x \left[ \int_0^t \left[ \left( \frac{-e_x}{1000 \bullet CC_{odb} \bullet C_E \bullet (44/12)} \right) \varepsilon(t') \right] y_x(t-t')dt' \right]}{\int_0^{TH} RF_{CO_2}(t)dt'} \right) \quad (11)$$

## 3. RESULTS

In the Top of Figure 1, the arithmetic means of the albedo of the different treatments from the field trial soil samples are shown. The gravimetric water content of the soil samples before drying was in the range of 25−36%. It should be noted that the soil samples were still quite wet (gravimetric water content: 15−27%) after drying. In the bottom of Figure 1, the arithmetic means of the different treatments of the albedo measurement for the pot trial series samples are shown. The gravimetric water content of these very dry soil samples was in the range of 0.1−0.4%. The standard errors indicated in the bottom of Figure 1 are lower compared to the standard errors indicated in the top of Figure 1. This can be partly explained by the fact that variations of field test samples are more heterogeneous compared to pot test samples. The maximum absolute difference in the arithmetic mean of the measured albedo values of the fresh (modestly dried) field trial soil samples was obtained between the control and the biochar-compost treatment which amounted to 0.0091 (0.0147).

The difference is slightly lower (0.0090 for wet soil samples and 0.011 for modestly dried soil samples) when the control is compared to the biochar treatment. For the dry pot trial series samples, the maximum difference obtained between the control and the biochar-compost 200 Mg/ha treatment (0.146) is much higher compared to the field trial soil samples. In general, all pot trial albedo values are much higher compared to the field trial samples which cannot be explained by the difference in

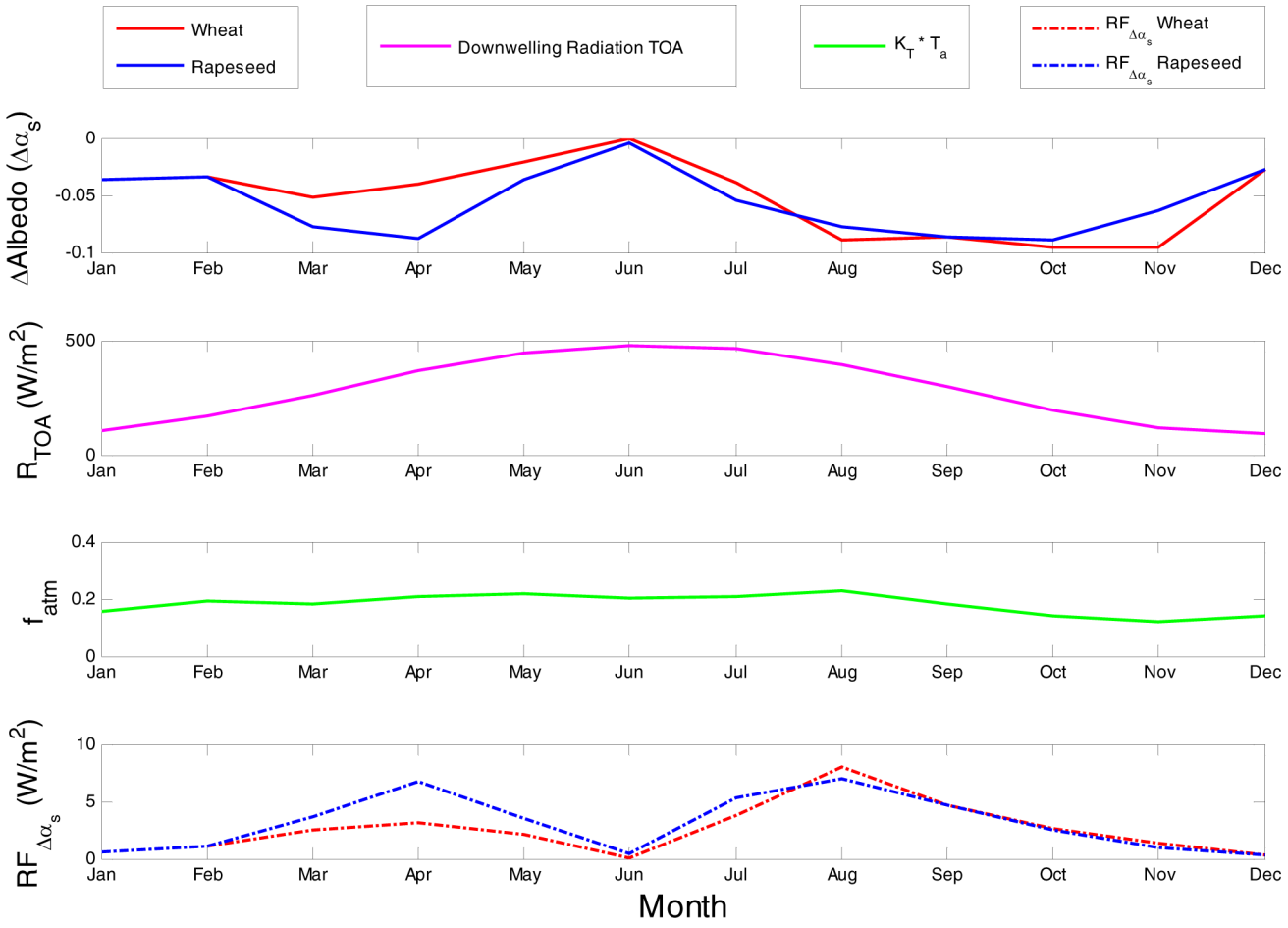


**Figure 2.** (Top) Monthly changes in surface albedo in the first year after biochar application to Wheat and Rapeseed fields near Donndorf, Germany. (Upper Middle) Monthly incoming solar radiation at the top of the atmosphere ("TOA"). (Lower Middle) Monthly mean two-way transmittance ("$f_{atm}$") of solar radiation throughout the atmosphere. (Bottom) Instantaneous local radiative forcing ("RF") associated with changes to surface albedo for the two cases (Annual mean RF is +3.1 W/m$^2$ for the rapeseed field and +2.6 W/m$^2$ for the wheat field). All graphs show the parameters for the same location.

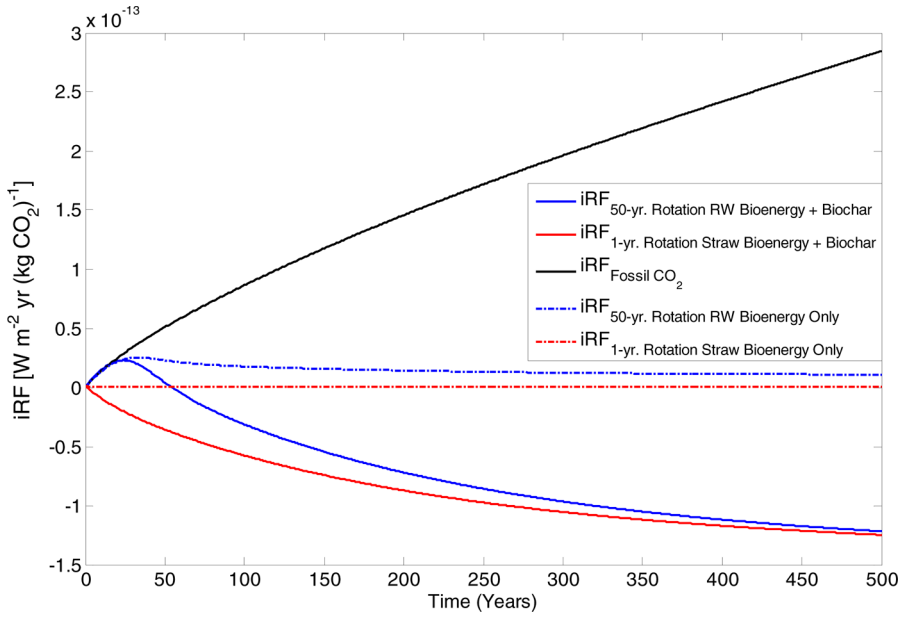


**Figure 3.** Time-integrated radiative forcing ("iRF") per 1 kg $CO_2$ pulse emission of bioenergy and biochar production compared to iRF per 1 kg $CO_2$ from stand-alone bioenergy production and to iRF per 1 kg $CO_2$ from fossil $CO_2$ emissions. Blue lines represent cases where 50 year rotation biomass is used as feedstock; red lines are used for cases where annual crops are used.

water contents alone: The albedo of the bright control soil of the pot trial is higher than the albedo of the darker control soil of the field trial. This is not surprising, as both albedo and color of soils are determined by surface properties.

In Figure 2, $\Delta\tilde{\alpha}_s$, $\Delta\tilde{R}_{TOA}$, $\tilde{f}_{Atm}$a, and $\widetilde{RF}_\alpha$ values resulting from the intra-annual delta albedo simulation for both wheat and rapeseed cultivation are presented.

The climax of vegetation coverage in June as well as the harvesting operations in the end of July and in August are clearly reflected in the top of Figure 2: While the dense vegetation cover cancels out any albedo differences of the soil in June, the biochar effect on the surface albedo change is evident after crop harvest and grubbing. Snow coverage reduces albedo differences in the winter months. Please note that the delta albedo decrease within in the first year (see eq 4) is not accounted for in Figure 2 to reduce the complexitiy for the interpretation of the graph.

If the biochar is applied to a wheat field (values for an application on a rapeseed field in brackets), the resulting GWP albedo characterization factors for a time horizon of 100 years are 0.14 (0.17) for a biochar feedstock with 50-year rotation period—roundwood (RW)—and 0.12 (0.14) for biochar feedstock with 1 year rotation period, straw. The GWP characterization factors resulting for 20 and 500 year time horizons are presented in SI Table S.3.

Figure 3 visualizes the (positive and negative) integrated radiative forcing caused by the temporal shift between biogenic $CO_2$ emissions during biochar/bioenergy production and the subsequent carbon sequestration in soil and vegetation.

Figure 3 reflects increases in the iRF due to the radiative forcing triggered by biogenic and fossil $CO_2$ emissions (upper part of the graph). The very low, but positive iRF of the straw bioenergy system is a result of the rapid absorption of the emitted carbon due to the fast regrowth of the annual crop. Decreases in the iRF displayed in the lower part of the figure result from the net removal of $CO_2$ from the atmosphere via carbon sequestration in soils. The derived GWP characterization factors of the combined bioenergy/biochar system for roundwood (values for straw in brackets) over a 100-year time horizon amount to −0.36 (−0.67) for biogenic $CO_2$ emissions and biogenic carbon stabilization, −0.04 (−0.04) for avoided fertilizer emissions and −0.14 (−0.14) for avoided soil $N_2O$ emission according to eqs 10 and 11. The GWP characterization factors resulting for 20 and 500 year time horizons are presented in SI Tables S5 and S6.

In Table 1, the synthesis of the overall results of our model is presented.

We compare the combined biochar-bioenergy system outlined above to a stand-alone bioenergy system—a biomass heating plant—which consumes the same amount of dry biomass feedstock. Regarding the stand-alone bioenergy system, we assume that 85% of the produced heat can be supplied into a district heating system with a high annual utilization factor of 75%, transport heat losses of 5%, and resulting lifecycle emissions saving of 0.254 kg $CO_2$e/kWh final energy (see UBA 2012[18]) due to the replacement of natural gas heating systems. In contrast to the biochar system, we assume that the biomass heating plant will not run at constant heat output throughout the year, but adapts the heat output to the heat demand in the district heating system. Thus, the stand-alone bioenergy system is assumed to produce not more than 5% of unusable waste heat. The specific lifecycle emissions from the construction of the biomass heating plant—if related to one ton of dry biomass input—were assumed to be equal to the life cycle emissions of the construction of a pyrolysis plant.

Table 2 indicates the overall result of our model:

**Table 1. Overall Climate Impact of the Biochar System for Wheat Cultivation (TH = 100)[a]**

| | feedstock | | |
|---|---|---|---|
| | straw | small round wood | |
| type of impact | Mg $CO_2$e/t DM | Mg $CO_2$e/t DM | indicated data based on |
| provision of biomass feedstock | 0.268 | 0.035 | ref 11 |
| transport of biomass to pyrolysis plants | 0.001 | 0.002 | ref 11 |
| emissions from the pyrolysis plant construction | 0.020 | 0.020 | ref 11 |
| heat offset | −0.328 | −0.315 | Section 2.1 |
| char transport to farm | 0.000 | 0.000 | ref 11 |
| char transport to fields | 0.001 | 0.001 | ref 11 |
| char application to soils | 0.000 | 0.000 | ref 11 |
| albedo impact for wheat field (rapeseed field) | 0.107 (0.124) | 0.128 (0.156) | SI Table S3 |
| temporal impact of biomass procurement losses | 0.000 | 0.033 | SI Table S4 |
| temp. impact of biochar system on carbon cycle | −0.595 | −0.330 | SI Tables S5, S6 |
| avoided fertilizer life cycle emissions | −0.034 | −0.034 | SI Tables S5, S6 |
| avoided soil $N_2O$ emissions | −0.124 | −0.128 | SI Tables S5, S6 |
| **overall impact for wheat field (rapeseed field)** | **-0.685 (−0.667)** | **-0.587 (−0.560)** | |

[a]Values for rapeseed cultivation are shown in parentheses.

**Table 2. Overall Climate Impact of the Stand-Alone Bioenergy System (TH = 100)**

| | feedstock | | |
|---|---|---|---|
| | straw | small round wood | |
| type of impact | Mg $CO_2$e/t DM | Mg $CO_2$e/t DM | indicated data based on |
| provision of biomass feedstock | 0.268 | 0.035 | ref 11 |
| transport of biomass to pyrolysis plants | 0.001 | 0.002 | ref 11 |
| emissions from the heating plant construction | 0.020 | 0.020 | Section 3 |
| heat offset | −1.084 | −1.041 | Section 3 |
| temporal impact of biomass procurement losses | 0.000 | 0.033 | SI Table S4 |
| temp. impact of bioenergy system on carbon cycle | 0.000 | 0.367 | SI Table S4 |
| **overall impact:** | **-0.795** | **-0.584** | |

## 4. DISCUSSION

While the absolute albedo of agricultural soils is strongly affected by the background soil type, the obtained differences in albedo values of treatments with the same background soil resulted mainly from the influence of biochar amendments, followed by the impact of compost amendments and varying soil water contents (see SI, Chapter 5). It is most reasonable to

compare the albedo values obtained from the soil samples from Donndorf with the values measured in Pistoia (18 months after biochar application) due to a similar amount of biochar application, similar background soils, same tilling depth and equal time period between biochar application and albedo measurement in both trials. However, the soils measured in Pistoia were very dry when analyzed as compared to the wet soils analyzed in Donndorf. The measurements of soil samples in Bayreuth resulted in larger absolute albedo differences when drier soil samples were compared. This is in line with the higher absolute soil albedo difference ($\Delta\alpha_{soil}$) measured on the dry soils in Pistoia as compared to the values obtained from the wet soil samples of Donndorf. The measured albedo differences are compared to published literature about biochar impacts on soil albedo and are discussed in greater detail in section 8 of the SI. Additional albedo field measurements on biochar sites under both wet and dry surface conditions in annual intervals would be helpful to complement the existing data and to better understand albedo development in time. It should be noticed in this context that the GWP albedo characterization factors are reduced by 1 order of magnitude if the delta albedo would completely vanish within two years after biochar application (see eq 4). Based on the modeled slow pyrolysis biochar system, we calculated that the overall climate impact of biochar systems is reduced by 13−22% due to the albedo impact of biochar application, depending on the type of biochar feedstock and crop cultivated on the soil. Since the albedo impact is linearly correlated to the field vegetation cover, agricultural systems with a large share of dense and year-round vegetation cover can minimize this impact. The albedo impact is also reduced when dark background soils are amended with biochar. To minimize the uncertainty connected to the modeling of the annual development of vegetation cover on basis of satellite data as carried out in this assessment, further field validations of the applied SDVI- methodology over heterogeneous surfaces divided into very small sections are necessary. In addition, further research should focus on the indirect impacts of albedo changes and the impacts of biochar application on the annual development of vegetation cover and near surface exchanges of water and energy. As $GWP_{albedo}$ is directly proportional to $T_a$, the monthly fraction of short wave radiation reaching TOA after reflection at the surface, it is very important to know realistic local $T_a$ values. Due to a lack of empirical measurements available, we estimated $T_a$ based on a simple one layer atmosphere model and average global values for short wave radiation absorption. If achievable, empirical measurements of $T_a$ would be very helpful to improve the assessment of $GWP_{albedo}$.

Due to the scarcity in globally available biomass (if biomass is used for biochar production, it cannot be used in standalone bioenergy systems to save fossil fuel emissions), we compared the climate impact of using one ton of dry wood (and straw respectively) in biochar systems and in stand-alone bioenergy systems. While we calculated overall $CO_2e$ emission savings with our model for both systems and feedstock types, bioenergy systems achieve 99−119% of the climate benefit of biochar systems according to our analysis. This can be mainly explained by the lower energy provision of the pyrolysis plant due to the lost energy contained in the biochar, the lower energy efficiency, and the lower heat use efficiency caused by the continuous operation of the pyrolysis plant. According to our assessment, a considerable fraction (23−29%) of the emissions savings of the biochar system is a result of avoided soil $N_2O$ emissions and avoided fertilizer life cycle emissions. Long-term measurements of avoided soil N2O emissions and more practical experience on the achievable fertilizer reductions after biochar application are necessary to reduce the uncertainty connected to this part of our assessment. The need to account for the climate impact of temporal shifts of the carbon cycle was clearly demonstrated by the assessment of both systems. Since we did not account for the impact of biochar application on biomass yields, soil methane emissions, soil inherent organic carbon content, and atmospheric soot concentration, additional research is necessary to complement the current assessment. If the biomass provision was to trigger indirect land use change via displacement effects, the resulting climate impact would have to be accounted for in the overall climate impact assessment. While this analysis focuses on a climate impact assessment, one should not loose sight of the opportunities of biochar application for soil amelioration.[38]

## ■ ASSOCIATED CONTENT

### Supporting Information

Additional information is vailabl including Figures S1 and S2 and Tables S1−S6. This material is available free of charge via the Internet at http://pubs.acs.org.

## ■ AUTHOR INFORMATION

### Corresponding Author

*Phone: 0049-176-23595765; e-mail: seppmeyer@gmx.de.

### Notes

The authors declare no competing financial interest.

## ■ ACKNOWLEDGMENTS

We thank the staff of the Department of Micrometeorology of the University of Bayreuth—special thanks go to Thomas Foken and Johannes Olesch—who generously supported us with time, advice, data and laboratory instruments to carry out the albedo analysis as well as Sascha Döring and Lydia Funke for their help with the field work and the laboratory measurements. In addition, S.M. thanks Anne and Uli for their support in difficult times. Finally, we thank our supervisors, NASA for free remote sensing information, the Landwirtschaftliche Lehranstalt Bayreuth and Carbon Terra for the test area and the charcoal needed for the field trial.

## ■ REFERENCES

(1) Glaser, B.; Birk, J. J. State of the scientific knowledge on properties and genesis of anthropogenic dark earths in central Amazonia (terra preta de Índio). *Geochim. Cosmochim. Acta* **2012**, *82*, 39−51.

(2) Libra, J. A.; Ro, K. S.; Kammann, C.; Funke, A.; Berge, N. D.; Neubauer, Y.; Titirici, M.-M.; Fuhner, C.; Bens, O.; Kern, J.; Emmerich, K.-H. Hydrothermal carbonization of biomass residuals: A comparative review of the chemistry, processes and applications of wet and dry pyrolysis. *Biofuels* **2011**, *2* (1), 71−106.

(3) Kammann, C.; Ratering, S.; Eckhardt, C.; Müller, C. Biochar and hydrochar effects on greenhouse gas (carbon dioxide, nitrous oxide, and methane) fluxes from soils. *J. Environ. Qual.* **2012**, *41*, 1052−1066.

(4) Singh, B.; Hatton, B.; Singh, B.; Cowie, A.; Kathuria, A. Influence of biochars on nitrous oxide emission and nitrogen leaching from two contrasting soils. *J. Environ. Qual* **2010**, *39*, 1224−1235.

(5) Steiner, C.; Glaser, B.; Geraldes Teixeira, W.; Lehmann, J.; Blum, W. E.; Zech, W. Nitrogen retention and plant uptake on a highly weathered central Amazonian Ferralsol amended with compost and charcoal. *J. Plant Nutr. Soil Sci.* **2008**, *171* (6), 893−899.

(6) Glaser, B.; Knorr, K.-H. Isotopic evidence for condensed aromatics from non-pyrogenic sources in soils—Implications for current methods for quantifying soil black carbon. *Rapid Commun. Mass Spectrom.* **2008**, *22* (7), 935−942.
(7) Liang, B.; Lehmann, J.; Sohi, S. P.; Thies, J. E.; O'Neill, B.; Trujillo, L.; Gaunt, J.; Solomon, D.; Grossman, J.; Neves, Ed. G.; Luizão, F. J. Black carbon affects the cycling of non-black carbon in soil. *Org. Geochem.* **2010**, *41* (2), 206−213.
(8) Meyer, S.; Glaser, B.; Quicker, P. Technical, economical, and climate-related aspects of biochar production technologies: A literature review. *Environ. Sci. Technol.* **2011**, *45* (22), 9473−9483.
(9) Genesio, L.; Miglietta, F.; Lugato, E.; Baronti, S.; Pieri, M.; Vaccari, F. P. Surface albedo following biochar application in durum wheat. *Environ. Res. Lett.* **2012**, *7* (1), 14025.
(10) Ramanathan, V.; Chung, C.; Kim, D.; Bettge, T.; Buja, L.; Kiehl, J. T.; Washington, W. M.; Fu, Q.; Sikka; Wild, M. Atmospheric brown clouds: Impacts on South Asian climate and hydrological cycle. *Proc. Natl. Acad. Sci. U.S.A.* **2005**, *102* (15), 5326.
(11) Hammond, J.; Shackley, S.; Sohi, S.; Brownsort, P. Prospective life cycle carbon abatement for pyrolysis biochar systems in the UK. *Energy Policy* **2011**, *39* (5), 2646−2655.
(12) Oguntunde, P. G.; Abiodun, B. J.; Ajayi, A. E.; van de Giesen, N. Effects of charcoal production on soil physical properties in Ghana. *J. Plant Nutr. Soil Sci.* **2008**, *171* (4), 591−596.
(13) Kirschbaum, M. U. F.; Whitehead, D.; Dean, S. M.; Beets, P. N.; Shepherd, J. D.; Ausseil, A.-G. E. Implications of albedo changes following afforestation on the benefits of forests as carbon sinks. *Biogeosciences* **2011**, *8* (12), 3687−3696.
(14) Bala, G.; Caldeira, K.; Wickett, M.; Phillips, T. J.; Lobell, D. B.; Delire, C.; Mirin, A. Combined climate and carbon-cycle effects of large-scale deforestation. *Pro. Natl. Acad. Sci.* **2007**, *104* (16), 6550−6555.
(15) Bright, R. M.; Cherubini, F.; Strømman, A. H. Climate impacts of bioenergy: Inclusion of carbon cycle and albedo dynamics in life cycle impact assessment. *Environ. Impact Assess. Rev.* **2012**, *37*, 2−11.
(16) Cherubini, F.; Peters, G. P.; Berntsen, T.; Strømman, A. H.; Hertwich, E. CO2 emissions from biomass combustion for bioenergy: Atmospheric decay and contribution to global warming. *GCB Bioenergy* **2011**, *3* (5), 413−426.
(17) Cholewa, T.; Siuta-Olcha, A. Comparison of heat losses in channel and preinsulated district heating networks. In *Environmental Engineering III*; Pawlowski, L., Dudzinska, Pawlowski, A., Eds.; CRC Press-Taylor & Francis Group: Boca Raton, FL, 2010; pp 569−574.
(18) Umweltbundesamt, Ökoinstitut e.V. ProBas: Prozessorientierte Basisdaten für Umweltmanagement-Instrumente. http://www.probas.umweltbundesamt.de/ (accessed April 4, 2012).
(19) Schulz, H.; Dunst, G.; Glaser, B. Synergistic biochar and compost effects on plant growth and properties of sandy and loamy substrates. *Agron. Sustain. Dev.* **2012**.
(20) Jiang, Z.; Huete, A. R.; Chen, J.; Chen, Y.; Li, J.; Yan, G.; Zhang, X. Analysis of NDVI and scaled difference vegetation index retrievals of vegetation fraction. *Remote Sens. Environ.* **2006**, *101* (3), 366−378.
(21) Oak Ridge National Laboratory Distributed Active Archive Center (ORNL DAAC). *MODIS Subsetted Land Products, Collection 5*; ORNL DAAC: Oak Ridge, TN, 2012; http://daac.ornl.gov/MODIS/modis.html (accessed February 17, 2012).
(22) Hochschule für Angewandte Wissenschaften FH München. Schneebedeckungsdauer zur Ertragsabschätzung und Auslegung von PV-Systemen basierend auf Satellitendaten von 2005 bis 2009. www-lse.ee.hm.edu/download/schneekarten_dach.pdf (accessed).
(23) Ramanathan, V.; Carmichael, G. Global and regional climate changes due to black carbon. *Nat. Geosci.* **2008**, *1* (4), 221−227, DOI: 10.1038/ngeo156.
(24) Cherubini, F.; Bright, R. M.; Strømman, A. H. Site-specific global warming potentials of biogenic $CO^2$ from bioenergy: Contributions from carbon fluxes and albedo dynamics. *Environ. Res. Lett.* **2012**.
(25) Muñoz, I.; Campra, P.; Fernández-Alba, A. R. Including CO2-emission equivalence of changes in land surface albedo in life cycle assessment. Methodology and case study on greenhouse agriculture. *Int. J. Life Cycle Assess.* **2010**, *15* (7), 672−681.
(26) Duffie, J. A.; Beckman, A. *Solar Engineering of Thermal Processes*, 2nd ed; John Wiley and Sons, Inc.: New York, 1991.
(27) Kalogirou, S. A. *Solar Energy Engineering Processes and Systems*; Elsevier, Academic Press: Burlington, MA, 2009.
(28) NASA. Surface Meteorology and Solar Energy (SSE) Release v.6.0. http://eosweb.larc.nasa.gov/cgi-bin/sse/sse.cgi (accessed March 27, 2012).
(29) Mani, T.; Murugan, P.; Mahinpey, N. Pyrolysis of oat straw and the comparison of the product yield to wheat and flax straw pyrolysis. *Energy Fuels* **2011**, *25* (7, SI), 2803−2807.
(30) Fu, Q.; Liou, K. N. Parameterization of the radiative properties of cirrus clouds. *J. Atmos. Sci.* **1993**, *50* (13), 2008−2025.
(31) Fu, Quiang, Liou, K. N. Fu-Liou online 200507 (Diurnal Simulation). http://snowdog.larc.nasa.gov/cgi-bin/rose/flp200503/sun/flsun.cgi (accessed April 4, 2012).
(32) Cherubini, F.; Guest, G.; Strømman, A. H. Application of probability distributions to the modeling of biogenic $CO_2$ fluxes in life cycle assessment. *GCB Bioenergy* **2012**, *4*, 784−798.
(33) Cherubini, F.; Strømman, A. H.; Hertwich, E. Effects of boreal forest management practices on the climate impact of CO2 emissions from bioenergy. *Ecol. Modell.* **2011**, *223* (1), 59−66.
(34) Joos, F.; Bruno, M. Pulse response functions are cost-efficient tools to model the link between carbon emissions, atmospheric CO2 and global warming. *Phys. Chem. Earth* **1996**, *21* (5−6), 471−476.
(35) Joos, F.; Prentice, I. C.; Sitch, S.; Meyer, R.; Hooss, G.; Plattner, G.-K.; Gerber, S.; Hasselmann, K. Global warming feedbacks on terrestrial carbon uptake under the Intergovernmental Panel on Climate Change (IPCC) emission scenarios. *Global Biogeochem. Cycles* **2001**, *15* (4), 891−907.
(36) Forster, P.; Venkatachalam, R. *Changes in Atmospheric Constituents and in Radiative Forcing. Fourth Assessment Report: Climate Change 2007: Working Group I Report: The Physical Science Basis*, Chapter 2; Geneva: IPCC, 2007.
(37) Woolf, D.; Amonette, J. E.; Street-Perrott, F. A.; Lehmann, J.; Joseph, S. Sustainable biochar to mitigate global climate change. *Nat Commun.* **2010**, *1*, 56.
(38) Fischer, Daniel, Glaser, Bruno. Synergisms between compost and biochar for sustainable soil amelioration. http://www.intechopen.com/books/management-of-organic-waste/synergism-between-biochar-and-compost-for-sustainable-soil-amelioration (accessed April 20, 2012).